NJC

ROYAL SOCIETY OF CHEMISTRY

PAPER

View Article Online
View Journal

Cite this: DOI: 10.1039/d6nj00414h

Split-type photoelectrochemical immunoassay for detecting carcinoembryonic antigen for colorectal cancer with ultrathin Bi_2MoO_6 nanosheets

Guowen Lu, *[ab] Yier Chou[b] and Zhongchen Liu*[a]

Received 2nd February 2026,
Accepted 10th March 2026

DOI: 10.1039/d6nj00414h

rsc.li/njc

Colorectal cancer is currently one of the most life-threatening gastrointestinal malignant tumors with high global morbidity and mortality, and carcinoembryonic antigen (CEA) is a clinically crucial biomarker for its screening and auxiliary diagnosis. Herein, a split-type photoelectrochemical (PEC) immunosensor for CEA detection was constructed using ultrathin Bi_2MoO_6 nanosheets (UBMO NSs) with strong and stable photocurrent as photoactive materials. This platform was integrated with an alkaline phosphatase (ALP)-mediated enzymatic catalytic amplification strategy for synergistic signal enhancement. In the presence of target CEA, a specific sandwich immunocomplex forms, and the ALP immobilized on the complex catalyzes L-ascorbic acid phosphate (AAP) hydrolysis to generate L-ascorbic acid (AA). As an efficient hole scavenger, AA promotes the separation of photogenerated electron–hole pairs in UBMO NSs, inducing a CEA concentration-dependent PEC signal enhancement. After systematic parameter optimization, the sensor exhibited a favorable linear response to CEA from 0.001 ng mL^{-1} to 100 ng mL^{-1} with a low limit of detection (LOD) of 0.43 pg mL^{-1}. It also maintained excellent performance in serially diluted human serum samples. Thus, this work provides a sensitive and reliable platform for clinical colorectal cancer screening.

Introduction

Carcinoembryonic antigen (CEA), a glycoprotein physiologically expressed during embryonic and fetal development, has emerged as a clinically pivotal biomarker for the diagnosis, prognosis assessment, and therapeutic monitoring of multiple malignant tumors – particularly colorectal cancer (including colon cancer and rectal cancer), as well as lung, breast, gastric, and pancreatic malignancies.[1,2] Rectal cancer, accounting for approximately 30–40% of all colorectal cancers, is a highly prevalent gastrointestinal malignancy with a global incidence on the rise, especially in developed regions.[3,4] For rectal cancer patients, serum CEA levels are elevated by 3–6 fold compared to healthy individuals in over 60% of cases, and this elevation is not only a critical indicator for distinguishing malignant tumors from benign gastrointestinal disorders but also post-operative recurrence in rectal cancer specifically, providing actionable insights for clinical decision-making. Notably, early-stage rectal and other colorectal cancer patients often exhibit only mild CEA elevation (5–10 ng mL^{-1}), which is challenging to differentiate from physiological fluctuations or benign conditions using conventional detection methods.[5,6] This limitation underscores the urgent need for sensors with ultra-low detection limits to enable early screening and diagnosis of rectal cancer, thereby improving patient survival rates. Against this backdrop, the development of highly sensitive, specific, and rapid CEA detection methodologies remains a pressing priority in clinical practice and translational oncology research.

Conventional techniques for CEA detection, such as enzyme-linked immunosorbent assay (ELISA), fluorescence (FL) and radioimmunoassay (RIA), have made substantial contributions to clinical diagnostics.[7–10] Nevertheless, these approaches are plagued by intrinsic limitations, such as cumbersome operational workflows, prolonged detection durations, high instrumentation costs, and potential environmental risks associated with radioactive labeling.[11,12] Given the urgent clinical need for rapid and sensitive detection of CEA, coupled with the inherent limitations of conventional methods, photoelectrochemical (PEC) sensing has emerged as a transformative alternative.[13–16] Its unique advantages are ideally suited to overcome the key challenges associated with quantifying CEA in complex biological matrices. As an innovative analytical technology that integrates photochemical and electrochemical principles, PEC sensing has attracted significant interest in biosensing due to

[a] School of Medicine, Tongji University, Shanghai 200331, China. E-mail: 1911339@tongji.edu.cn
[b] Thyroid and Breast Surgery Department, The Affiliated People's hospital of Ningbo University, Ningbo 315040, China. E-mail: 13860184888@163.com

its distinct advantages, including low background noise, exceptional sensitivity, simplified instrumentation, and rapid readout.[17–19] The underlying mechanism involves the generation of photoelectrons and holes by photoactive materials upon light irradiation, triggering a photocurrent signal that can be regulated by specific biomolecular interactions at the sensing system. This unique signal transduction mechanism effectively minimizes non-specific interference and significantly enhances the signal-to-noise ratio compared to conventional electrochemical techniques. Consequently, PEC-based biosensors have emerged as a highly promising tool for the sensitive detection of various biomarkers.

To fully realize the potential of PEC sensing for CEA detection, the selection of photoactive materials is dependent on efficient visible-light absorption, rapid photogenerated charge separation and transfer kinetics, and excellent biocompatibility for biological applications. Among the diverse array of semiconductor materials, bismuth molybdate (Bi_2MoO_6) has emerged as a compelling candidate for PEC applications, owing to its optimal band gap energy ($\sim$2.8 eV), outstanding chemical stability under physiological conditions, inherent biocompatibility, and efficient visible-light-driven photocatalytic activity.[20,21] In contrast to traditional wide-band-gap semiconductors, which are limited to ultraviolet light excitation, Bi_2MoO_6 can harness a broader portion of the solar spectrum, thereby alleviating reliance on costly UV light sources and significantly broadening its practical utility in ambient light conditions.[22,23] Despite these favorable properties, the application of Bi_2MoO_6 in CEA-specific PEC immunosensing remains underexplored, especially the application of an ultrathin nanosheet structure, leaving a critical gap in the development of high-performance CEA biosensors. To address this limitation, we adjusted the structure of Bi_2MoO_6 into ultrathin nanosheets through dimensional optimization. This strategy not only mitigates the inherent charge recombination issue of bulk Bi_2MoO_6 but also enhances the biomolecule loading capacity, which is essential for specific antibody–antigen interactions at the sensing interface.[24–26] More importantly, the ultrathin structure enables enhanced light absorption through multiple internal reflections within the nanosheets, further optimizing the utilization of incident light and boosting photocurrent generation. Collectively, this approach effectively addresses the inherent limitations of existing CEA-PEC sensors, which predominantly rely on traditional wide-band-gap semiconductors or thick-layer structures, characterized by narrow light response ranges, sluggish charge transfer kinetics, and limited biomolecule loading capacity.

In this study, we report the development of a novel split-type PEC immunosensor based on ultrathin Bi_2MoO_6 nanosheets (UBMO NSs) for the sensitive and specific detection of CEA, a core biomarker for colorectal cancer screening and auxiliary diagnosis (Scheme 1). This split-type configuration is chosen primarily for its dual advantages of effective background suppression and flexible signal amplification. The spatial separation of the immunoreaction from the photoelectrode prevents surface fouling, while enabling efficient solution-phase enzymatic amplification. The UBMO NSs are synthesized *via* a scalable hydrothermal approach and employed as the core photoactive layer of the PEC sensing platform. Upon the formation of a CEA-mediated sandwich immunocomplex,

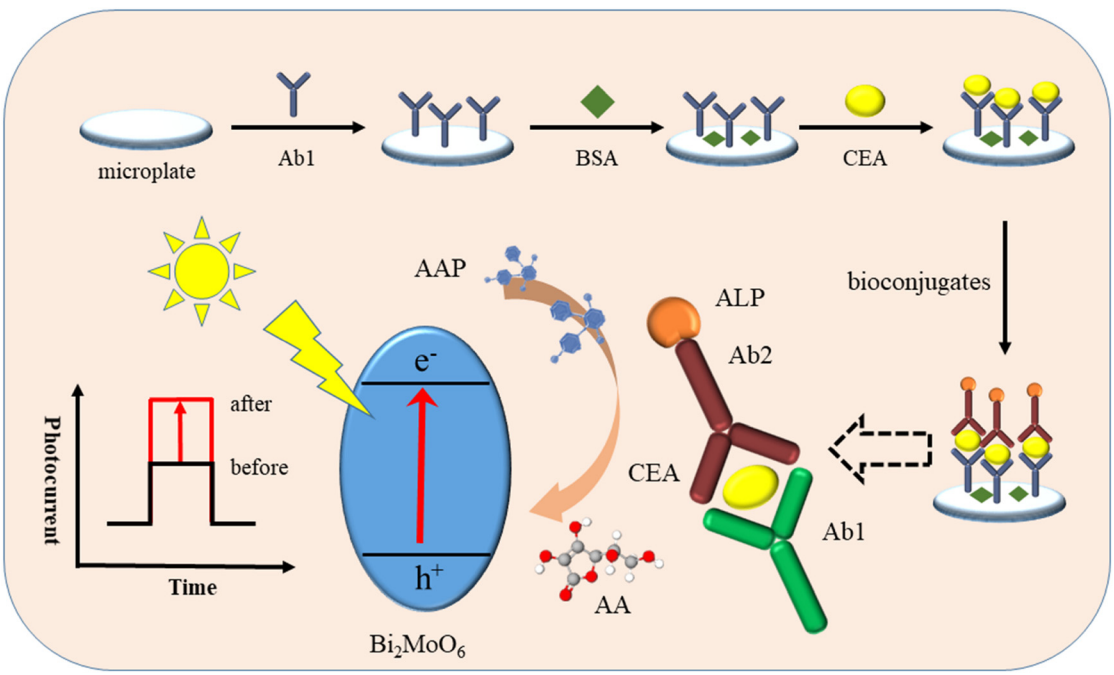

Scheme 1 Schematic illustration of the ALP-assisted PEC immunoassay for CEA detection (Ab1: capture antibody; BSA: bovine serum albumin; CEA: carcinoembryonic antigen; Ab2: detection antibody; AA: L-ascorbic acid; ALP: alkaline phosphatase; AAP: L-ascorbic acid phosphate; bioconjugates: ALP-Ab2).

ALP-labeled detection antibodies (ALP-Ab2) are introduced into the sensing system. ALP then specifically catalyzes the hydrolytic conversion of AAP to AA. As an efficient hole scavenger, the generated AA effectively suppresses the recombination of photogenerated electron–hole pairs in UBMO NSs and accelerates interfacial charge transfer, thereby eliciting a pronounced enhancement of the PEC photocurrent signal. Consequently, the photocurrent intensity exhibits a distinct dose-dependent increase with rising CEA concentration, establishing a robust quantitative basis for accurate CEA quantification. This work not only addresses a critical gap in the application of UBMO NSs for CEA-targeted PEC sensing but also proposes a reliable and practical strategy for constructing clinically translatable PEC immunosensing platforms, which paves a new way for early clinical diagnosis of colorectal cancer.

Experimental section

Chemicals and reagents

Bovine serum albumin (BSA), $Na_2MoO_4{\cdot}2H_2O$, thioacetamide (TAA), CTAB, aminopropyltriethoxysilane (APTES), and *N*-hydroxysuccinimide (NHS) were obtained from Aladdin Reagent Co., Ltd. Alpha-fetoprotein (AFP), monoclonal mouse anti-human carcinoembryonic antigen CEA antibody (Ab1; clone number: CB30; cat#: ab35657), polyclonal rabbit anti-human CEA antibody (Ab2; cat#: ab131070), CEA standards (cat#: ab264604), prostate-specific antigen (PSA), and CEA ELISA kits were purchased from Abcam. $Bi(NO_3)_3{\cdot}5H_2O$, AAP, glutamic acid (Glu), AA, ALP, 1-(3-dimethylaminopropyl)-3-ethylcarbodiimide hydrochloride (EDC·HCl), immunoglobulin G (IgG), cardiac troponin I (cTnI), ethylene glycol, and other chemicals were obtained from Sigma-Aldrich.

Synthesis of ultrathin Bi_2MoO_6 nanosheets (UBMO NSs)

To prepare ultrathin UBMO NSs, 200 mg of CTAB ($\geq$99%), 1 g of $Na_2MoO_4{\cdot}2H_2O$ (analytical grade), and 4 g of ($Bi(NO_3)_3{\cdot}5H_2O$ ($\geq$98%) were dissolved sequentially in 300 mL of a mixed solvent (ultrapure water/ethylene glycol, v/v = 1 : 1) under magnetic stirring to ensure complete dissolution and formation of a homogeneous precursor solution. Subsequently, the well-dispersed precursor was then sealed into a 500 mL Teflon autoclave and heated to 170 °C in a muffle furnace for 12 h. After the reaction, the resulting product was harvested and rinsed thoroughly with absolute ethanol for 3 cycles to remove unreacted precursors and residual solvent. Finally, the collected precipitate was dried to obtain pure UBMO NSs. For the preparation of bulk Bi_2MoO_6 as a reference sample, the above synthetic procedure was replicated exactly, with the sole modification of omitting CTAB from the precursor mixture.

Preparation of ALP-Ab2

This experiment adopted the EDC/NHS activation method for conjugating anti-CEA antibody with ALP. The procedure is as follows: First, the antibody was desalted by a 10 kDa ultrafiltration tube and reconstituted in 0.05 M PBS (pH 6.0, the optimal pH for carboxyl activation). ALP was dissolved in 0.05 M Tris–HCl buffer for renaturation at 37 °C for 10 min, then cooled to 4 °C. Freshly prepared EDC/NHS solution was added to the antibody, and the mixture was gently stirred in an ice bath for 30 min to activate carboxyl groups. The activated antibody was added dropwise to the ALP solution at an antibody-to-ALP mass ratio of 3 : 1, and conjugation was performed at 4 °C in the dark for 4 h under pH 8.0 conditions to prevent ALP inactivation. BSA was then added to block unreacted active sites and terminate the reaction. Finally, the target ALP-antibody conjugate (ALP-Ab2) was collected after 4 rounds of centrifugal purification with a 10 kDa ultrafiltration tube to remove unreacted reagents and impurities.

Fabrication of the PEC sensing system

UBMO NS powder was dispersed in ultrapure water *via* ultrasonic treatment to prepare a homogeneous dispersion (2.0 mg mL^{-1}). Subsequently, 20 μL of this pre-dispersed solution was drop-cast onto the designated region of FTO conductive glass, yielding the UBMO NSs/FTO electrode.

The fabrication of the sandwich-type immunosensing platform was conducted as follows: initially, 100 μL of the primary antibody (Ab1, 20 μg mL^{-1}) was added to microplates and incubated at 4 °C for 24 h, followed by rinsing with a washing buffer (10 mM PBS containing 0.05% Tween 20). Next, the Ab1-coated microplates were blocked with 300 μL of blocking buffer (10 mM PBS with 1.0 wt% BSA) at 37 °C for 2 h to eliminate non-specific binding sites. After discarding the blocking solution, 100 μL of CEA standard solutions with gradient concentrations were added to the microplates, and the mixture was incubated at 37 °C for 30 min under mild shaking; the microplates were then rinsed thoroughly using the aforementioned washing buffer. Thereafter, 100 μL of the ALP-Ab2 solution was pipetted into the microplates and incubated at 37 °C for 30 min, allowing the formation of sandwich-type immunocomplexes on the microplate surface. After another round of washing, 100 μL of 50 mM AAP substrate solution was added to each microplate. Finally, after enzymatic hydrolysis at 25 °C for 20 min, the resulting reaction solution was transferred into a detection cell for subsequent photoelectrochemical measurements.

Compliance with ethical standards

All experiments were performed in accordance with the Guidelines of Tongji University and Ningbo University (China) and approved by the ethics committees of Tongji University and Ningbo University (China). Informed consent was obtained from human participants involved in this study.

Results and discussion

Characterization of UBMO NSs

To elucidate the crystal structure and lattice parameters of the as-synthesized UBMO NSs, X-ray diffraction (XRD) characterization was conducted. As presented in Fig. 1A, the diffraction profile of UBMO NSs is in excellent conformity with the standard orthorhombic Bi_2MoO_6 phase (JCPDS Card No. 21-0102),

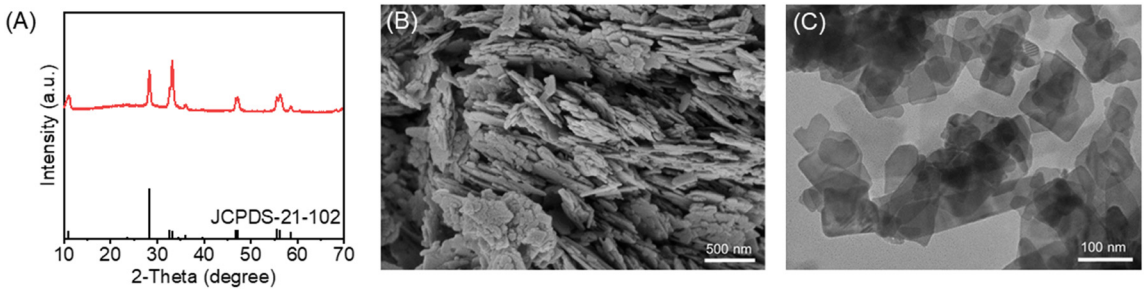

Fig. 1 (A) XRD pattern, (B) SEM image and (C) TEM image of UBMO NSs.

confirming its phase purity and structural integrity.[27] The well-resolved diffraction peaks at 10.8°, 28.2°, 32.5°, 33.1°, 46.8°, and 47.1° are indexed to the (0 2 0), (1 1 3), (2 0 0), (0 6 0), (2 0 2), and (2 6 0) crystal planes, respectively. Their sharpness indicates high crystallinity – an essential prerequisite for efficient photogenerated charge separation and transport, which underpins the superior PEC performance.

The morphological features, especially the ultrathin lamellar characteristic of the UBMO NSs, were comprehensively probed *via* scanning electron microscopy (SEM) and transmission electron microscopy (TEM). The SEM micrograph (Fig. 1B) demonstrates that UBMO NSs possess a uniformly dispersed sheet-like morphology with no apparent agglomeration, manifesting favorable structural homogeneity. More critically, the TEM image (Fig. 1C) explicitly reveals the ultrathin 2D lamellar architecture of the UBMO NSs, with a thickness ranging from sub-nanometer to nanometer scale. This observation is consistent with the SEM result, collectively confirming the successful fabrication of ultrathin 2D UBMO NSs with the desired structural features. Furthermore, the expanded electrode–electrolyte interface derived from the ultrathin structure facilitates efficient interfacial charge transfer kinetics, which directly enhances the PEC response intensity, laying a pivotal foundation for the construction of high-sensitivity PEC immunosensing platforms.

Feasibility evaluation

To implement the designed PEC bioassay, the AA-induced amplified PEC signals were investigated *via* transient photocurrent response measurements. As shown in Fig. 2A, the photocurrent of the UBMO NSs reaches 206.5 nA without AA treatment, nearly twice that of bulk Bi_2MoO_6. After AA incubation, this value surges dramatically to 664.1 nA, confirming the superior light-harvesting capacity of the 2D UBMO NSs over 3D bulk Bi_2MoO_6 and validating AA as an efficient hole scavenger. Electrochemical impedance spectroscopy (EIS) measurements (Fig. 2B) were performed to corroborate these findings. The unmodified FTO electrode shows a small charge transfer resistance (R_{ct}) of 53.3 Ω, while the bulk 3D Bi_2MoO_6-modified FTO exhibits the largest R_{ct} (836.7 Ω). In contrast, UBMO NS-modified FTO presents a much smaller semicircle with a reduced R_{ct} of 298.8 Ω. The EIS results are highly consistent with photocurrent data, consistently demonstrating the superior charge transfer kinetics of the UBMO NS-based photoelectrodes. A key validation was to confirm AA generation after the sandwich immune reaction between CEA and its specific antibodies. As shown in Fig. 2C, the PEC signal remains at the blank control level without target CEA, whereas a significant PEC signal enhancement is observed in its presence. Collectively, these findings verify the successful construction of the UBMO NS-based PEC biosensing platform *via* a sandwich enzymatic catalysis strategy, which has been preliminarily proven to be feasible for the quantitative detection of CEA.

Optimization of the experimental conditions

To optimize the analytical performance of the PEC biosensor, we investigated three key parameters, including the volume of photosensitive material solution, antigen–antibody incubation time, and AAP catalytic time. As the core component for photoelectric conversion in the PEC sensing system, the photoactive substrate exerts a decisive effect on photocurrent intensity

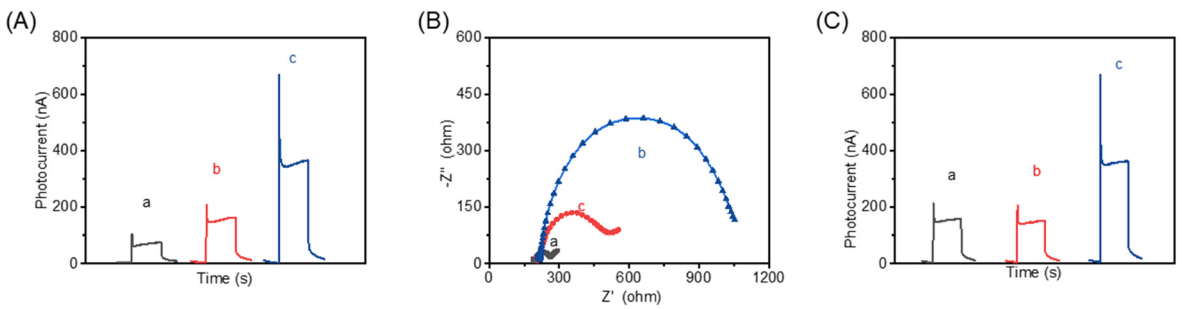

Fig. 2 (A) PEC responses of (a) bulk 3D Bi_2MoO_6, and UBMO NSs (b) without or (c) with AA. (B) Nyquist diagrams of (a) unmodified FTO, (b) bulk 3D Bi_2MoO_6/FTO and (c) UBMO NSs/FTO. (C) PEC responses of (a) blank, (b) Ab1 + ALP-Ab2 + AAP, and (c) Ab1 + ALP-Ab2 + AAP + CEA (100 ng mL^{-1}).

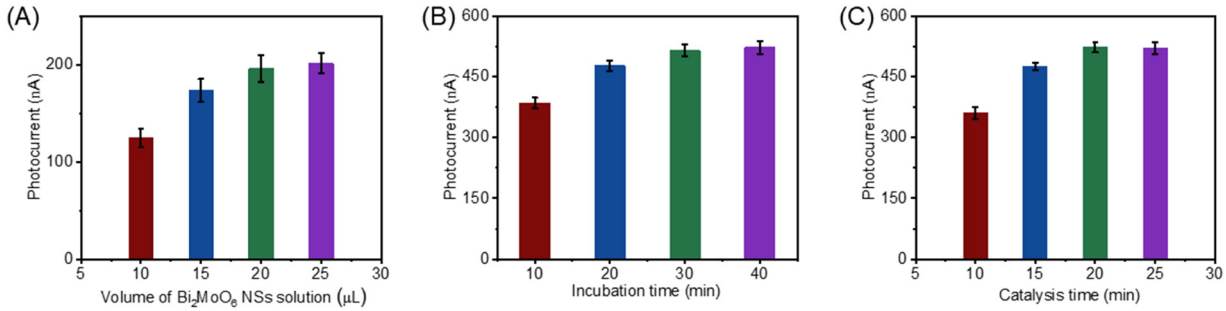

Fig. 3 Effects of (A) UBMO NS solution volume, (B) incubation time and (C) catalytic time on the signal intensity of the UBMO NS-based PEC immunoassay.

modulation, with the dosage of UBMO NS solution directly correlating to the final photocurrent output. An insufficient volume lacks adequate active sites for an optimal PEC response, while an excessively high volume causes nanomaterial agglomeration and elevates detection costs unnecessarily. A systematic investigation was thus conducted, and the platform exhibited the strongest PEC response at 20 μL of the UBMO NS solution, which was set as the optimal dosage. Subsequently, the effects of two time-dependent parameters on the sensing performance were explored, as shown in Fig. 3B and C, respectively. Fig. 3B characterizes the correlation between immunoreaction time and photocurrent intensity, while Fig. 3C depicts the PEC response trend with ALP-catalyzed AAP reaction time. For the immunoreaction time, the photocurrent rises gradually with extended incubation due to sufficient antigen–antibody specific binding, plateauing at 30 min when the reaction is complete. For the AAP catalytic time, the photocurrent increases steadily as ALP continuously hydrolyzes AAP to generate photoactive products, reaching a stable plateau at 20 min upon catalytic equilibrium. Accordingly, 30 min and 20 min were set as the optimized immunoreaction incubation time and ALP-mediated AAP catalytic time for the PEC sensing platform, respectively.

Responses of the proposed PEC immunoassay

Under the optimized experimental conditions, the analytical performance of the UBMO NSs-based PEC biosensor was evaluated by investigating the correlation between the recorded PEC signal responses and CEA levels. As shown in Fig. 4A, the photocurrent intensity exhibits a distinct positive correlation with CEA levels within the linear range of 0.001 to 100 ng mL^{-1}. Linear fitting of the experimental data yields the regression equation: I (nA) = 89.19 × lg $C_{[CEA]}$ + 460.87 (R^2 = 0.9883) with a LOD of 0.43 pg mL^{-1}. Notably, this LOD is well below the critical threshold for clinical CEA detection, fully meeting the practical requirements of clinical diagnostic assays. Furthermore, a comparative analysis with previously reported CEA sensing platforms confirms that the proposed biosensor exhibits superior analytical performance (Table 1), which highlights its prominent advantages in CEA quantification.

Real biological samples typically comprise a complex matrix of diverse components, which necessitates excellent selectivity as a fundamental prerequisite for biosensors to realize accurate target detection. To evaluate the specificity of the constructed PEC immunoassay, detection signals were measured after incubating the sensing platform with common interfering biomolecules (PSA, AFP, Glu, IgG and cTnI), with the results presented in Fig. 4B. Comparative analysis from each interference group reveals that the presence of these coexisting biomolecules induced only negligible fluctuations in the photocurrent intensity. In contrast, a prominent photocurrent response is observed in the presence of the target (10 ng mL^{-1}). These results demonstrate the outstanding specificity of the developed UBMO NS-based PEC immunoassay, which is capable of selectively recognizing CEA against complex biological matrix interferences.

Meanwhile, by quantifying the photocurrent decay during different storage periods, the long-term stability of the biosensor was evaluated, which is one of the important prerequisites for its practical clinical application. As depicted in Fig. 4C, the

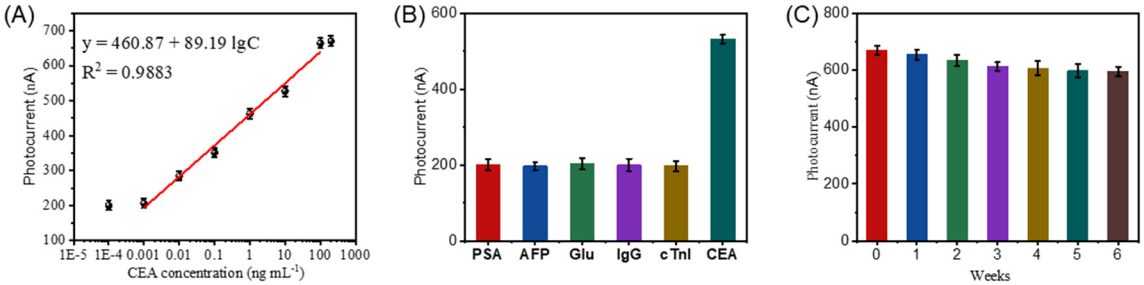

Fig. 4 (A) Calibration curve, (B) selectivity and (C) long-term stability of the proposed PEC immunoassay.

Table 1 Comparison of different methods

Methods	Materials	Linear range (ng mL^{-1})	LOD (ng mL^{-1})	Ref.
PEC	Anthocyanin-sensitized poly(indole-5-carboxylic acid)	0.01–500	0.0033	28
FL	Eu-MOF	0.1–20	0.012	29
PEC and photothermal	Ag/MoO_3-Pd	0.01–50	0.026	30
Electrochemiluminescence	Luminol on streptavidin-coated gold nanoparticle	5–300	2.51	31
Electrochemical	Nitrogen-rich mesoporous carbon	0.0094–1000	0.0094	32
PEC	UBMO NSs	0.001–100	0.00043	This work

Table 2 Practical application of the UBMO NS-based PEC biosensor

Sample no.	Method; concentration: mean ± SD (U mL^{-1}, n = 3)		t_{exp}
	By PEC immunoassay	By ELISA kit	
1	1.05 ± 0.11 (4.4%)	0.97 ± 0.09 (2.5%)	0.81
2	5.06 ± 0.22 (3.2%)	5.11 ± 0.25 (2.1%)	1.41
3	10.03 ± 0.29 (4.9%)	10.15 ± 0.33 (5.3%)	1.53
4	15.22 ± 0.43 (5.7%)	15.13 ± 0.37 (3.6%)	1.62
5	20.18 ± 0.62 (8.4%)	20.27 ± 0.59 (6.9%)	1.93

photocurrent intensity exhibits gradual attenuation with extended storage time, yet all observed reductions fall within an acceptable range of variation. Notably, the biosensor retains 88.80% of its initial level even after six weeks of storage. These results conclusively validate the excellent long-term stability of the developed PEC biosensor, further supporting its feasibility for practical applications.

Monitoring of complex biological matrices

Furthermore, to validate the practical applicability of the UBMO NS-based PEC biosensing method for complex biological matrices, human serum samples were further analyzed in parallel *via* the developed PEC assay and a commercial ELISA kit, with the comparative results summarized in Table 2. Statistical analysis reveals that the calculated t_{exp} values for all serum samples were lower than the critical value ($t_{crit[0.05,4]}$ = 2.78). This finding confirms that the proposed PEC immunoassay is a reliable and practical approach for the quantitative determination of CEA in complex biological samples.

Conclusions

In summary, a PEC immunosensor for quantitative CEA detection was successfully constructed by combining UBMO NSs with an immunoenzymatic signal amplification strategy. Experimental characterizations confirm that 2D UBMO NSs have markedly enhanced light-harvesting capacity and accelerated photogenerated charge separation compared to bulk 3D Bi_2MoO_6, providing a robust photoelectric foundation for high-sensitivity PEC sensing. The CEA-triggered bioenzymatic catalytic system designed here shows excellent specificity and feasibility. ALP is efficiently immobilized on pretreated microplate wells *via* CEA-induced antigen–antibody immune complexes. Upon AAP addition, ALP catalyzes its hydrolysis to generate AA, which acts as an efficient hole scavenger to capture photogenerated holes of UBMO NSs. This process ultimately achieves a CEA concentration-dependent enhancement of the PEC signal. The UBMO NS-based PEC immunosensor exhibits superior analytical performance, including a wide linear range, a low LOD meeting clinical early CEA detection requirements, outstanding selectivity against interfering biomolecules, and favorable long-term stability. It also realizes accurate and reliable CEA quantification in complex human serum samples, with performance comparable to commercial ELISA kits. Collectively, this work develops a cost-effective, practical and sensitive PEC strategy for CEA detection, which offers a promising analytical system for the early diagnosis of CEA-related malignancies with notable translational biomedical potential.

Author contributions

Guowen Lu: conceptualization, methodology, visualization, investigation, and writing – review and editing. Yier Chou: writing – review and editing and project administration. Zhongchen Liu: methodology, funding acquisition, supervision, writing – review and editing, and project administration.

Conflicts of interest

There are no conflicts to declare.

Data availability

Data will be made available upon request.

Supplementary information (SI) is available. See DOI: https://doi.org/10.1039/d6nj00414h.

Acknowledgements

This research was funded by the Talent Initiation Fund of Tongji University (2021XRC01).

References

1 L. Wang, W. Hong, D. Fan, J. Lin, Z. Liu, M. Fan, X. Lin, D. Lin and S. Feng, *Nanoscale*, 2025, **17**, 16349–16360.
2 Z. Lin, M. Zhai, H. Wang, M. Li, L. Liu, P. Zhang, L. Yan, H. Liu, K. Tao and T. Zhang, *Cancer Lett.*, 2025, **611**, 217442.
3 C. Yeh, M. C. Wheless, K. K. Ciombor and A. Cercek, *Annu. Rev. Med.*, 2026, **77**, 177–192.
4 H. Li, F. Wang, X. Zhang, B. Liang, Y. Chen, Y. Chenxiang, Q. Liao, F. Xue, D. Wang and B. He, *Sens. Actuators, B*, 2026, **446**, 138700.

5 Y. Yuan, Y. Di, Y. Chen, H. Yu, R. Li, S. Yu, F. Li, Z. Li and Y. Yin, *Anal. Methods*, 2024, **16**, 1225–1231.
6 S. Lu, D. Chen, Y. Shu, X. Wang, Y. Fan, Y. Qu and W. Jin, *Nanoscale*, 2025, **17**, 26828–26834.
7 L. Guo, B. Li, S. W. Wong, M. Chen, Q. Xu, L. Ge and H. F. Kwok, *Biosens. Bioelectron.*, 2023, **236**, 115404.
8 R. Zeng, Y. Li, Y. Li, Q. Wan, Z. Huang, Z. Qiu and D. Tang, *Research*, 2022, **2022**, 9831521.
9 Y. Cheng, Y. Li, H. Ren, B. Wen, W. Liang, S. Zhang, B. Cong, M. Jiang and C. Hong, *Sens. Actuators, B*, 2024, **405**, 135381.
10 R. Li, D. Fu, X. Yuan, G. Niu, Y. Fan, J. Shi, Y. Yang, J. Ye, J. Han, Y. Kang and X. Ji, *Small*, 2024, **20**, 2404741.
11 R. Zeng, W. Wang, G. Cai, Z. Huang, J. Tao, D. Tang and C. Zhu, *Nano Energy*, 2020, **74**, 104931.
12 R. Zeng, J. Tao, D. Tang, D. Knopp, J. Shu and X. Cao, *Nano Energy*, 2020, **71**, 104580.
13 R. Zeng, Z. Huang, Y. Wang and D. Tang, *ChemElectroChem*, 2020, **7**, 1537–1541.
14 R. Zeng, H. Gong, Y. Li, Y. Li, W. Lin, D. Tang and D. Knopp, *Anal. Chem.*, 2022, **94**, 7442–7448.
15 R. Zeng, L. Zhang, L. Su, Z. Luo, Q. Zhou and D. Tang, *Biosens. Bioelectron.*, 2019, **133**, 100–106.
16 K. Xiao, R. Zhu, C. Du, H. Zheng, X. Zhang and J. Chen, *Anal. Chem.*, 2022, **94**, 9844–9850.
17 R. Zeng, J. Xu, L. Lu, Q. Lin, X. Huang, L. Huang, M. Li and D. Tang, *Chem. Commun.*, 2022, **58**, 7562–7565.
18 R. Zeng, J. Xu, T. Liang, M. Li and D. Tang, *ACS Sens.*, 2023, **8**, 317–325.
19 R. Zeng, L. Zhang, Z. Luo and D. Tang, *Anal. Chem.*, 2019, **91**, 7835–7841.
20 F. Li, M. Li, H. Wang, X. Wang, L. Zheng, D. Guan, L. Chang, J. Xu and Y. Wang, *Adv. Mater.*, 2022, **34**, 2107826.
21 Y. Zheng, T. Zhou, X. Zhao, W. K. Pang, H. Gao, S. Li, Z. Zhou, H. Liu and Z. Guo, *Adv. Mater.*, 2017, **29**, 1700396.
22 R. Zeng, T. Liu, M. Qiu, H. Tan, Y. Gu, N. Ye, Z. Dong, L. Li, F. Lin, Q. Sun, Q. Zhang, L. Gu, M. Luo, D. Tang and S. Guo, *J. Am. Chem. Soc.*, 2024, **146**, 9721–9727.
23 R. Zeng, K. Lian, B. Su, L. Lu, J. Lin, D. Tang, S. Lin and X. Wang, *Angew. Chem., Int. Ed.*, 2021, **60**, 25055–25062.
24 R. Zeng, Q. Gao, L. Xiao, W. Wang, Y. Gu, H. Huang, Y. Tan, D. Tang and S. Guo, *J. Am. Chem. Soc.*, 2024, **146**, 10023–10031.
25 J. Di, X. Zhao, C. Lian, M. Ji, J. Xia, J. Xiong, W. Zhou, X. Cao, Y. She, H. Liu, K. P. Loh, S. J. Pennycook, H. Li and Z. Liu, *Nano Energy*, 2019, **61**, 54–59.
26 Y. Xie, X. Shang, D. Liu, H. Zhao, Y. Gu, Z. Zhang and X. Wang, *Appl. Catal., B*, 2019, **259**, 118087.
27 J. Xu, R. Zeng, L. Huang, Z. Qiu and D. Tang, *Anal. Chem.*, 2022, **94**, 11441–11448.
28 Y. Cheng, J. Wang, L. Zheng, J. Zhang, D. Liu and G. Nie, *Sens. Actuators, B*, 2025, **422**, 136681.
29 S. Zhang, Y. Luo, W. Zhuang, G. Zhong, L. Su, T. Xu and X. Zhang, *Anal. Chem.*, 2023, **95**, 18739–18747.
30 L. Lu, X. Hu, R. Zeng, Q. Lin, X. Huang, Q. Wei, D. Tang and D. Knopp, *Biosens. Bioelectron.*, 2023, **230**, 115267.
31 M. Mohammadniaei, M. Zhang, X. Qin, W. Wang, L. Pia, H. Gürbüz, S. H. Helalat, M. Naseri and Y. Sun, *Talanta*, 2024, **266**, 125087.
32 D. Mehta, S. Kaur and T. C. Nagaiah, *Anal. Methods*, 2024, **16**, 1473–1479.